International Forum on Aeroelasticity and Structural Dynamics
IFASD 2017
25-28 June 2017 Como, Italy

APPLICATION OF LOW-ORDER WAKE INFLOW MODELS TO ROTORCRAFT AEROMECHANICS

Serafini J[1], Cardito F[1], Bernardini G[1], Gennaretti M[1]

[1]Department of Engineering
University Roma Tre
Via della Vasca Navale 79, 00144, Roma, Italy
serafini@uniroma3.it
felice.cardito@uniroma3.it
g.bernardini@uniroma3.it
m.gennaretti@uniroma3.it

Keywords: helicopter flight dynamics, dynamic wake inflow, reduced-order modeling.

Abstract: The effect of dynamic inflow modeling on helicopter aeromechanic simulation for stability, response and control purposes is investigated. Two different linear time-invariant inflow models, extracted from high-fidelity aerodynamic simulations, are presented and applied. One provides the wake inflow as a function of rotor kinematic variables, while the second one gives the wake inflow dynamics forced by rotor loads. In both cases, first the involved transfer functions are identified through time-marching aerodynamic simulations, and then a rational-matrix formula is applied for their finite-state approximation. The resulting state-space dynamic inflow models are applied to helicopter response and stability analyses, showing that the aeromechanic transfer functions and poles predicted by kinematic-based and loads-based models are somewhat different, with those related to the loads-based inflow depending on the kinematic perturbation considered to synthesize the model. Both simulations present discrepancies with respect to those obtained by the widely-used Pitt-Peters dynamic inflow model.

1 INTRODUCTION

Dynamic wake inflow modeling plays a fundamental role in the development of efficient and reliable computational tools for aeromechanic analysis of rotorcraft. Indeed, it allows the evaluation of blade downwash and hence aerodynamic loads through sectional formulations, without introducing complex CFD solvers. It is worth noting that, although the inflow models are usually derived introducing a potential velocity description of the flow field, they can be effectively coupled with sectional load formulations which consider non-potential phenomena like static or dynamic stall, as shown, for instance, in [1] where the link between blade loads, wake vorticity and inflow is analyzed in detail.

Analytical models, like the well-known Pitt-Peters and Peters-He ones [2, 3], are yet widely used for dynamic inflow evaluation, due to their ease of implementation. However, they may suffer from low accuracy when the approximations they are based on are not acceptable for the problem under consideration. For instance, it has been observed that, due to change of tip vortex-blade relative position in roll and pitch motions, actual off-axis helicopter response may be of opposite sign with respect to numerical prediction provided by the original Pitt-Peters model, which is unable to capture such phenomenon (see [4] for review and details). Other

flight conditions for which standard analytical inflow models might prove to be not enough accurate include those concerning vortex ring state, windmill brake and autorotation [5–7], or those where interactional effects between main rotor and tail rotor, fuselage or ground play a relevant role [8, 9].

Although some of these issues have been addressed with suitable tailoring (and increased complexity) of the analytical models, "gray areas" in the determination of helicopter response through analytical inflow are still present. Thanks to the increase of computational power, in the last years, the numerical identification of dynamic inflow models as Reduced Order Models derived from High-Fidelity aerodynamic solvers has become an interesting alternative to widely-applied analytical formulations [10]. In this case, the level of accuracy of the inflow model corresponds to that of the numerical predictions, with the possibility of including aerodynamic effects that could not be considered through analytical formulations. Obviously, this is obtained at the cost of determining an inflow model for each specific flight configuration/condition of interest.

In the recent past, the authors developed a technique for extracting linear dynamic inflow models from time-marching simulations [11, 12]. Exploiting the capability of a boundary-integral-equation aerodynamic solver for potential flows to simulate aerodynamics of arbitrary body configurations in arbitrary motion, it has been applied also to coaxial rotors [13, 14] and to in-ground-effect flight conditions [15]. Higher-order radial and azimuthal inflow descriptions have been introduced, as well [14, 16]. Two types of dynamic inflow models have been introduced, one relating inflow to rotor kinematic degrees of freedom and one relating inflow to rotor loads (similarly to Pitt-Peters and Peters-He models).

The aim of this paper is the assessment of these dynamic inflow models when applied for flight dynamics simulations, with particular attention to helicopter stability and response. Next, inflow reduced-order modelling and helicopter dynamics modelling applied are briefly outlined, and then the results of stability and response analysis concerning a medium-weight helicopter are discussed.

2 DYNAMIC INFLOW MODELING

Akin to the formulation introduced in [2, 17], the distribution of the modelled approximated wake inflow perturbation over the rotor disc, λ_{app}, is expressed by the following linear interpolation formula, defined in a non-rotating polar coordinate system, (r_c, ψ),

$$\lambda_{app}(r_c, \psi, t) = \lambda_0(t) + r_c \left[\lambda_s(t)\, \sin\psi + \lambda_c(t)\, \cos\psi\right] \tag{1}$$

where r_c denotes distance from the disc center, ψ is the azimuth angular distance from the rear position, whereas the coefficients, λ_0, λ_s and λ_c represent, respectively, mean value, side-to-side gradient and fore-to-aft gradient time evolutions.

As proposed in [11], the dynamic model is extracted by a multi-step procedure: it starts with the application of a high-fidelity aerodynamic solver to evaluate blade wake inflow corresponding to chirp-type perturbations about a steady trimmed flight condition and in a given frequency range of interest, of the flight dynamics variables (namely, those related to hub motion, blade flapping components, blade pitch control); next, the FFT of these outputs provides samples of the transfer function matrix, $\boldsymbol{H}$, such that, in the Laplace domain,

$$\tilde{\boldsymbol{\lambda}} = \boldsymbol{H}(s)\, \tilde{\boldsymbol{q}} \tag{2}$$

with $\boldsymbol{\lambda} = \{\lambda_0\ \lambda_s\ \lambda_c\}^T$ and $\boldsymbol{q}$ collecting hub motion components (linear velocity, $\boldsymbol{q}_v = \{u\ v\ w\}^T$ and angular velocity, $\boldsymbol{q}_\Omega = \{p\ q\ r\}^T$, components) , blade flapping components, $\boldsymbol{q}_\beta = \{\beta_0\ \beta_s\ \beta_c\}^T$, and blade pitch controls, $\boldsymbol{q}_\theta = \{\theta_0\ \theta_s\ \theta_c\}^T$.

The final step of the finite-state wake inflow model identification process consists in deriving rational forms providing the best fit of the transfer functions sampled in the frequency domain, followed by transformation into time domain. Specifically, from the application of a least-square procedure assuring the stability of the identified poles, the transfer function, $\boldsymbol{H}$, is described through the following rational-matrix approximation (RMA) form [18]

$$\boldsymbol{H} = s\boldsymbol{A}_1^{wi} + \boldsymbol{A}_0^{wi} + \boldsymbol{C}^{wi}[s\boldsymbol{I} - \boldsymbol{A}^{wi}]^{-1}\boldsymbol{B}^{wi} \tag{3}$$

where $\boldsymbol{A}_1^{wi}$, $\boldsymbol{A}_0^{wi}$, $\boldsymbol{A}^{wi}$, $\boldsymbol{B}^{wi}$ and $\boldsymbol{C}^{wi}$ are real, fully populated matrices, and s denotes the Laplace-domain variable. Matrices $\boldsymbol{A}_1^{wi}$ and $\boldsymbol{A}_0^{wi}$ have dimensions $[3 \times 12]$, $\boldsymbol{A}^{wi}$, is a $[N_a \times N_a]$ matrix containing the N_a poles of the rational expression, $\boldsymbol{B}^{wi}$, is a $[N_a \times 12]$ matrix, and $\boldsymbol{C}^{wi}$ has dimensions $[3 \times N_a]$. Then, combining Eq. 2 with Eq. 3 and transforming into time domain yields the following finite-state model relating the wake inflow coefficients to the kinematic variables of interest

$$\begin{aligned} \boldsymbol{\lambda} &= \boldsymbol{A}_1^{wi}\,\dot{\boldsymbol{q}} + \boldsymbol{A}_0^{wi}\,\boldsymbol{q} + \boldsymbol{C}^{wi}\,\boldsymbol{x} \\ \dot{\boldsymbol{x}} &= \boldsymbol{A}^{wi}\,\boldsymbol{x} + \boldsymbol{B}^{wi}\,\boldsymbol{q} \end{aligned} \tag{4}$$

where $\boldsymbol{x}$ is the vector of the additional states representing wake inflow dynamics. Further details on the rational matrix approximation technique applied are given in [18].

2.1 Inflow model based on rotor loads

Starting from the above modelling technique, it is possible to develop an alternative procedure which provides a dynamic model relating the inflow coefficients to rotor loads perturbations. It requires the additional identification of the transfer function matrix, $\boldsymbol{G}$, between the perturbations of the kinematic variables ($\boldsymbol{q}_v, \boldsymbol{q}_\Omega, \boldsymbol{q}_\theta$ or $\boldsymbol{q}_\beta$) and the corresponding rotor thrust, roll moment and pitch moment, $\boldsymbol{f} = \{C_T, C_L, C_M\}^T$. This is obtained through a procedure similar to that described above, simply replacing the aerodynamic output $\boldsymbol{\lambda}$ with $\boldsymbol{f}$ (as available from the same aerodynamic time responses used for the identification of the matrix $\boldsymbol{H}$) [11].

To this purpose, the model is determined by perturbing one of the kinematic variable subsets of interest. Considering, for instance, blade control pitch perturbations, $\boldsymbol{q}_\theta$, once the relations $\tilde{\boldsymbol{\lambda}} = \boldsymbol{H}_\theta\,\tilde{\boldsymbol{q}}_\theta$ and $\tilde{\boldsymbol{f}} = \boldsymbol{G}_\theta\,\tilde{\boldsymbol{q}}_\theta$ have been identified, for each sampling frequency the wake inflow coefficients are directly related to the rotor loads by the expression

$$\tilde{\boldsymbol{\lambda}} = \hat{\boldsymbol{H}}_\theta \tilde{\boldsymbol{f}} \tag{5}$$

where $\hat{\boldsymbol{H}}_{\boldsymbol{\theta}} = \boldsymbol{H}_\theta \boldsymbol{G}_\theta^{-1}$ is a 3×3 matrix (equivalent transfer function matrices, $\hat{\boldsymbol{H}}_v$,$\hat{\boldsymbol{H}}_\Omega$ and $\hat{\boldsymbol{H}}_\beta$ may be derived from $\boldsymbol{G}_v$,$\boldsymbol{G}_\Omega$ and $\boldsymbol{G}_\beta$).

Then, the following RMA is applied to the sampled values of $\hat{\boldsymbol{H}}_{\boldsymbol{\theta}}$,

$$\hat{\boldsymbol{H}}_{\boldsymbol{\theta}} = \boldsymbol{C}^{wi}[s\boldsymbol{I} - \boldsymbol{A}^{wi}]^{-1}\boldsymbol{B}^{wi} \tag{6}$$

where $\boldsymbol{A}^{wi}$ is a $[N_a \times N_a]$, $\boldsymbol{B}^{wi}$ is a $[N_a \times 3]$ matrix, and $\boldsymbol{C}^{wi}$ has dimensions $[3 \times N_a]$. In this case, the polynomial part of the RMA has been omitted in that, the examination of the

asymptotic behavior of the transfer functions between wake inflow and loads provided by any unsteady aerodynamic operator reveals that it tends to zero as perturbation frequency tends to infinity [14]. Clearly, equivalent dynamic inflow models may be determined by considering the RMA of matrices $\hat{\boldsymbol{H}}_v$,$\hat{\boldsymbol{H}}_\Omega$ and $\hat{\boldsymbol{H}}_\beta$ instead of $\hat{\boldsymbol{H}}_\theta$.

Finally, Eq. 6 is transformed into time domain, yielding a state-space representation of the inflow coefficients with respect to a set of rotor loads perturbations [11].

$$\begin{aligned} \boldsymbol{\lambda} &= \boldsymbol{C}^{wi}\,\boldsymbol{x} \\ \dot{\boldsymbol{x}} &= \boldsymbol{A}^{wi}\,\boldsymbol{x} + \boldsymbol{B}^{wi}\,\boldsymbol{f} \end{aligned} \tag{7}$$

3 HELICOPTER SIMULATION TOOL

The *HELISTAB* code is a comprehensive helicopter code developed in the last decade at Roma Tre University. It considers rigid body dynamics, blade aeroelasticity, airframe elastic motion, as well as effects from actuators dynamics and stability augmentation systems. Passive and active pilot models are included, and both linear and nonlinear analyses may be performed. *HELISTAB* has been validated and applied within the activities of the European Project ARISTOTEL, addressed to the study of Rotorcraft-Pilot Couplings phenomena [19–22].

The linearized equations of aeromechanics are written as a first order differential system,

$$\dot{\boldsymbol{z}} = \boldsymbol{A}\boldsymbol{z} + \boldsymbol{B}\boldsymbol{u} \tag{8}$$

where $\boldsymbol{z}$ collects Lagrangian coordinates of elastic blade and airframe deformations and their derivatives, airframe rigid-body (center-of-mass) linear and angular velocity components, Euler angles and inflow states, $\boldsymbol{x}$, whereas $\boldsymbol{u}$ collects main and tail rotor controls and their first and second order derivatives, namely, $\boldsymbol{u}^T = \{\ddot{\theta}_0\,\dot{\theta}_0\,\theta_0\,\ddot{\theta}_s \ldots \theta_p\}$.

In the following, details concerning the derivation of matrices $\boldsymbol{A}$ and $\boldsymbol{B}$ in Eq. 8 are provided for aeromechanics formulations using both kinematic-based and loads-based dynamic inflow models.

3.1 Kinematic-based inflow

Recasting the vector of state variables as $\boldsymbol{z}^T = \{\boldsymbol{y}^T\ \boldsymbol{x}^T\}$, coupling the rotor and airframe dynamics equations with the dynamic inflow model of Eq. 4 yields the following aeromechanics model

$$\begin{aligned} \dot{\boldsymbol{y}} &= \boldsymbol{A}_y\boldsymbol{y} + \boldsymbol{C}_\lambda\boldsymbol{\lambda} + \boldsymbol{B}_y\boldsymbol{u} \\ \boldsymbol{\lambda} &= \boldsymbol{A}^{wi}_{1y}\dot{\boldsymbol{y}} + \boldsymbol{A}^{wi}_{0y}\boldsymbol{y} + \boldsymbol{C}^{wi}\boldsymbol{x} + \boldsymbol{A}^{wi}_{0u}\boldsymbol{u} \\ \dot{\boldsymbol{x}} &= \boldsymbol{B}^{wi}_{y}\boldsymbol{y} + \boldsymbol{A}^{wi}\boldsymbol{x} + \boldsymbol{B}^{wi}_{u}\boldsymbol{u} \end{aligned} \tag{9}$$

where $\boldsymbol{C}_\lambda$ collects the derivatives of the aerodynamic generalized forces of the aeromechanic model with respect to $\boldsymbol{\lambda}$. In addition, the matrices of the wake inflow model in Eq. 9 are obtained by re-organization of those in Eq. 4, in order to be consistent with the vectors of variables defined for the aeromechanic model (for instance, hub linear velocities considered in Eq. 4 are given as a combination of the airframe dofs considered in the vector $\boldsymbol{y}$).

Then, substituting the inflow model in the rotor/airframe dynamics equations yields the following set of first-order differential equations governing the helicopter dynamics

$$\begin{aligned}\dot{\boldsymbol{y}} &= \left(\boldsymbol{I} - \boldsymbol{C}_\lambda \boldsymbol{A}_{1y}^{wi}\right)^{-1}\left[\left(\boldsymbol{A}_y + \boldsymbol{C}_\lambda \boldsymbol{A}_{0y}^{wi}\right)\boldsymbol{y} + \boldsymbol{C}_\lambda \boldsymbol{C}^{wi}\boldsymbol{x} + \left(\boldsymbol{B}_y + \boldsymbol{C}_\lambda \boldsymbol{A}_{0u}^{wi}\right)\boldsymbol{u}\right] \\ \dot{\boldsymbol{x}} &= \boldsymbol{B}_y^{wi}\boldsymbol{y} + \boldsymbol{A}^{wi}\boldsymbol{x} + \boldsymbol{B}_u^{wi}\boldsymbol{u}\end{aligned} \tag{10}$$

from which matrices $\boldsymbol{A}$ and $\boldsymbol{B}$ of Eq. 8 may be readily identified.

3.2 Load-based inflow

When load-based inflow model is applied, the aeromechanics equations may be written as

$$\begin{aligned}\dot{\boldsymbol{y}} &= \boldsymbol{A}_y\boldsymbol{y} + \boldsymbol{C}_\lambda\boldsymbol{\lambda} + \boldsymbol{B}_y\boldsymbol{u} \\ \boldsymbol{\lambda} &= \boldsymbol{C}^{wi}\boldsymbol{x} \\ \dot{\boldsymbol{x}} &= \boldsymbol{A}^{wi}\boldsymbol{x} + \boldsymbol{B}_f^{wi}\boldsymbol{f}\end{aligned} \tag{11}$$

where the perturbative hub loads appearing in Eq. 11 are given by the following linearized form

$$\boldsymbol{f} = \boldsymbol{F}_y\boldsymbol{y} + \boldsymbol{F}_\lambda\boldsymbol{\lambda} + \boldsymbol{F}_u\boldsymbol{u} \tag{12}$$

Finally, combining Eq. 11 with Eq. 12 yields the following set of first-order differential equations governing the helicopter dynamics

$$\begin{aligned}\dot{\boldsymbol{y}} &= \boldsymbol{A}_y\boldsymbol{y} + \boldsymbol{C}_\lambda\boldsymbol{C}^{wi}\boldsymbol{x} + \boldsymbol{B}_y\boldsymbol{u} \\ \dot{\boldsymbol{x}} &= \boldsymbol{B}_f^{wi}\boldsymbol{F}_y\boldsymbol{y} + \left(\boldsymbol{A}^{wi} + \boldsymbol{B}^{wi}\boldsymbol{F}_\lambda\boldsymbol{C}^{wi}\right)\boldsymbol{x} + \boldsymbol{B}_f^{wi}\boldsymbol{F}_u\boldsymbol{u}\end{aligned} \tag{13}$$

from which matrices $\boldsymbol{A}$ and $\boldsymbol{B}$ of Eq. 8 may be readily identified.

4 NUMERICAL RESULTS

In this section, results concerning the validation of the state-space wake inflow models are first presented, followed by the application to rotorcraft aeromechanic problems.

The dynamic inflow models are determined through application of a high-fidelity aerodynamic solver consisting of a Boundary Element Method (BEM) tool for potential-flow solutions [23]. It is suited for rotors in arbitrary motion and is capable of accurate simulations taking into account free-wake and aerodynamic interference effects in multi-body configurations (like coaxial rotors or rotor-fuselage systems), as well as severe blade-vortex interactions.

The test case examined concerns a mid-weight helicopter model inspired to the Bo-105, in hovering flight condition, whose main data are reported in table 1.

4.1 Inflow transfer functions

In Fig. 1 the transfer function relating λ_0, to blade collective pitch, θ_0, is shown. Specifically, it presents the comparison between the sampled values evaluated by the BEM aerodynamic solver and the predictions by the RMA. In the frequency range examined, their agreement is excellent, thus proving the high level of accuracy of the RMA. Moreover, the high value of the corresponding evaluated coherence parameter [24] demonstrates the good quality of the identification process applied.

mass	$2200\ kg$
I_{xx}	$1430\ kg\,m^2$
I_{yy}	$4975\ kg\,m^2$
I_{zz}	$4100\ kg\,m^2$
I_{xz}	$650\ kg\,m^2$
MR type	hingeless
MR radius	$4.91\ m$
MR chord	$0.27\ m$
MR angular speed	$44.4\ rad/s$
MR blade twist	$-8\,^\circ/m$
MR number of blades	4
TR radius	$1\ m$
TR chord	0.2 m
TR angular speed	$230\ rad/s$
TR number of blades	2

Table 1: Main helicopter data

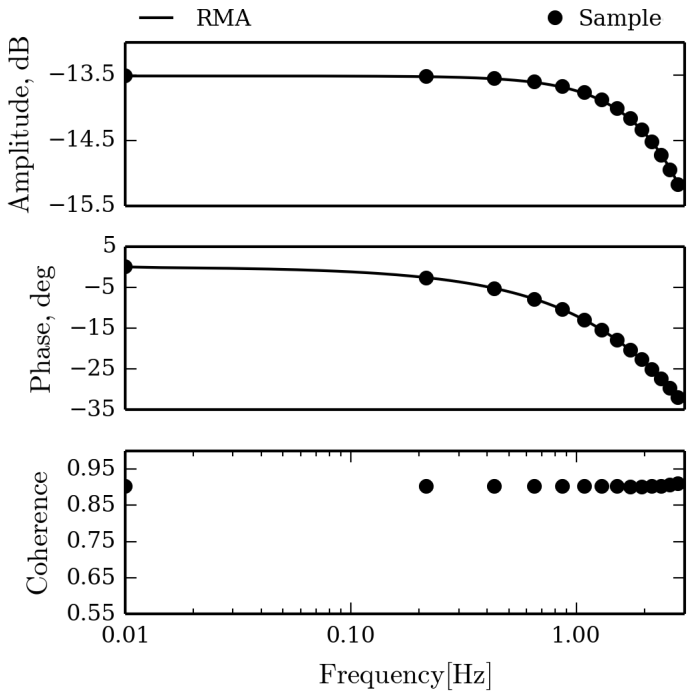

Figure 1: Transfer function λ_0 vs θ_0.

Next, considering the loads-based inflow modeling, Figs. 2, 3 and 4 present the transfer functions respectively relating, λ_0 to thrust coefficient, C_T, and λ_s to roll and pitch moment coefficients C_L and C_M, respectively. Specifically, the transfer functions appearing in $\boldsymbol{H}_\theta$,$\boldsymbol{H}_v$,$\boldsymbol{H}_\Omega$ and $\boldsymbol{H}_\beta$ are compared, along with that given by the well known Pitt-Peters dynamic inflow model (indicated as PP) [2, 17]. Note that, due to the axial symmetry of hovering flight condition, the transfer function relating λ_c to C_M is coincident with the one relating λ_s to C_L. Likewise, the transfer function relating λ_c to C_L is coincident with that relating λ_s to C_M.

These figures confirm the capability of the RMA technique to provide excellent analytical ap-

proximations of the sampled transfer functions. They demonstrate also that the loads-based inflow model is significantly dependent on the kinematic perturbations it is derived from (linear velocity, angular velocity, pitch control or blade flapping variables). As already observed in [12], this behavior is explained by the fact that the inflow depends on wake vorticity and hence on the bound vorticity distribution (strictly related to the lift coefficient distribution) which, in turn, is heavily affected by the downwash distribution.

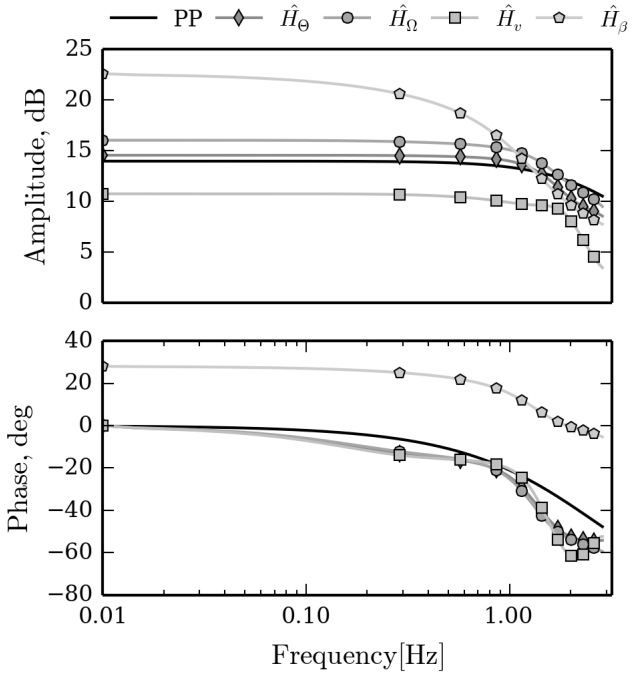

Figure 2: Transfer function λ_0 vs C_T.

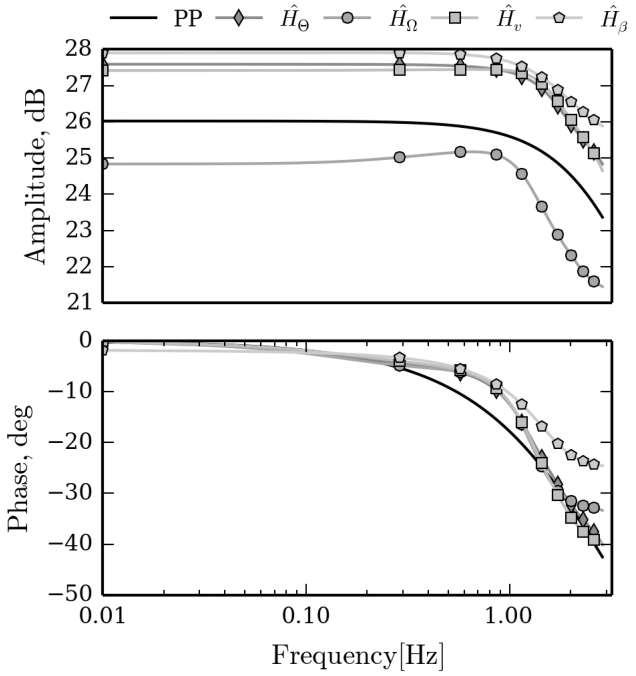

Figure 3: Transfer function λ_s vs C_L.

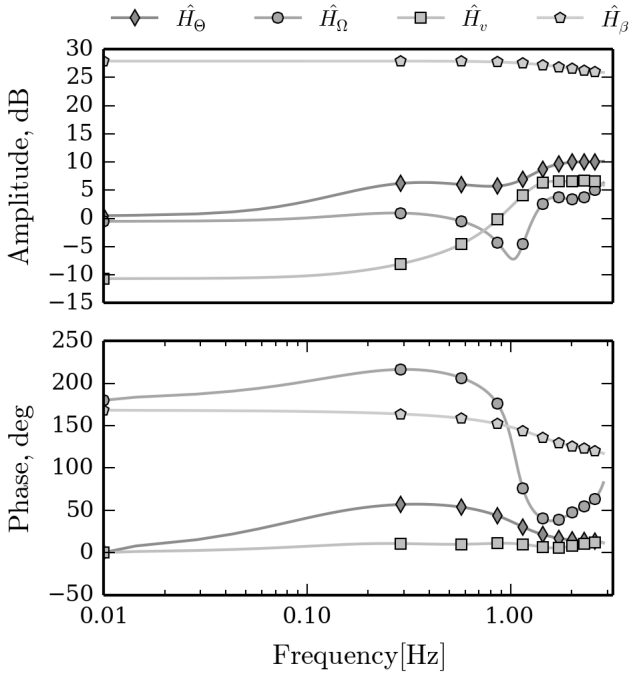

Figure 4: Transfer function λ_s vs C_M.

Moreover, it is interesting to observe that, differently from the Pitt-Peters model, the off-diagonal transfer function, λ_s to C_M, determined by the high-fidelity aerodynamic solver does not vanish (relevant values close to those of the λ_s to C_L transfer function are even present in the $\hat{\boldsymbol{H}}_\beta$ matrix). This coupling term is somehow expected considering that the model is derived by a free wake aerodynamic solver, capable of taking into account wake distortion effects.

Since developed for flight dynamics simulation purposes, a low-frequency-range transfer function approximation is pursued. For aeroelastic applications a more detailed time-periodic inflow distribution model is required [14, 16].

4.2 Helicopter aeromechanics

Then, the effect of the different inflow models considered on helicopter dynamics prediction is assessed.

First, the effect of the wake inflow models considered on aeromechanics eigenvalues and eigenvectors is examined. Figures 5 and 6 show the poles of the aeromechanics transfer functions provided by the kinematic-based wake inflow model ($\boldsymbol{H}_q^{ae}$), the loads-based inflow models derived through four different kinematic perturbations ($\boldsymbol{H}_\theta^{ae}$, $\boldsymbol{H}_\Omega^{ae}$, $\boldsymbol{H}_v^{ae}$, $\boldsymbol{H}_\beta^{ae}$), and the Pitt-Peters model.

Relevant differences may be observed on some of the poles, and specifically those related to phugoid, roll-pitch oscillations, roll subsidence, dutch roll, spiral and heave subsidence modes (Figs. 7 and 8 depict the magnitude of the most relevant components of the eigenvectors associated to the flight dynamics poles, as obtained by the Pitt-Peters inflow). Note that, also low-frequency aeroelastic poles (regressive lag and regressive flap), since coupled with flight dynamics modes, are affected by wake inflow model change.

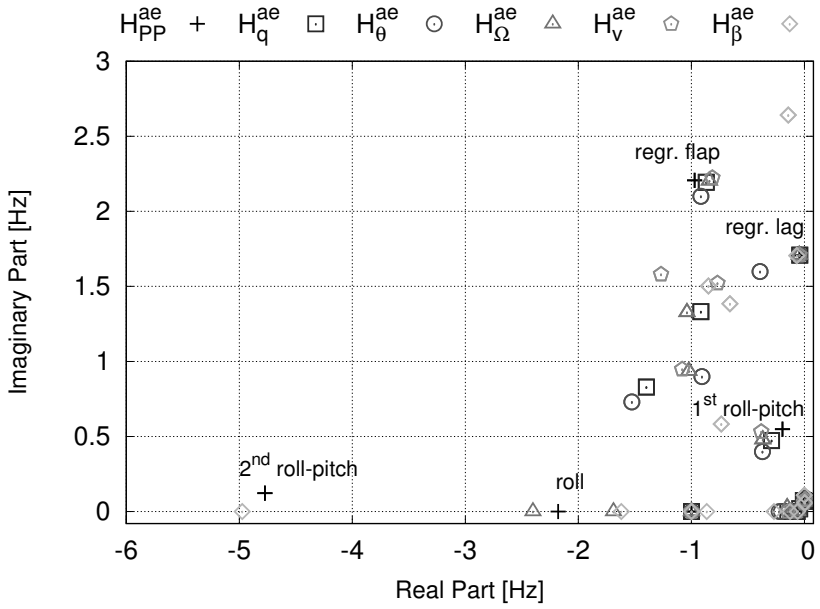

Figure 5: Aeromechanics roots determined by different inflow models.

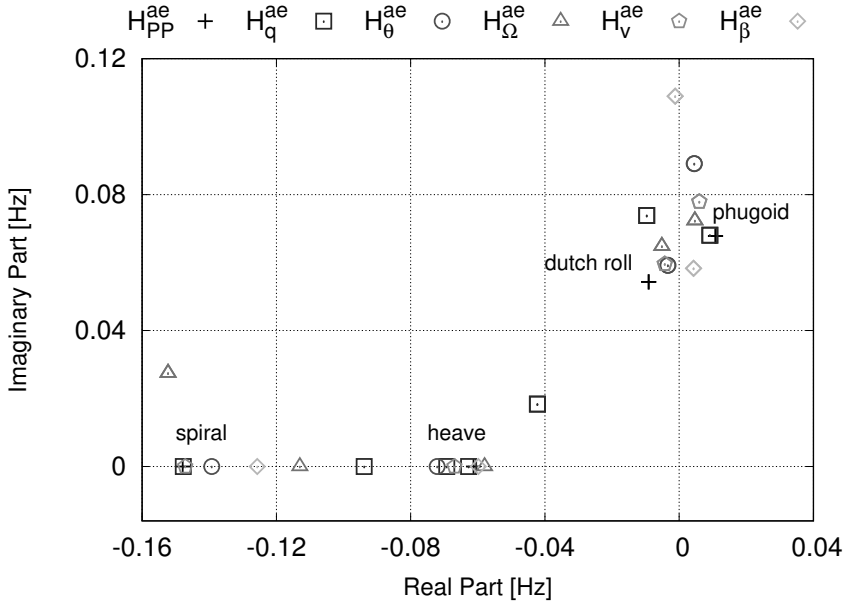

Figure 6: Aeromechanics roots determined by different inflow models, detail.

Finally, the main aeromechanics transfer functions are examined in detail. Figures 9 to 13 depict five transfer functions, respectively w vs θ_0, q vs θ_s, p vs θ_c, r vs θ_p and p vs θ_s (with θ_p denoting tail rotor collective pitch), each evaluated through application of the kinematic-based wake inflow model ($\boldsymbol{H}^{ae}_{q}$), the loads-based inflow models introduced ($\boldsymbol{H}^{ae}_{\theta}$, $\boldsymbol{H}^{ae}_{\Omega}$, $\boldsymbol{H}^{ae}_{v}$, $\boldsymbol{H}^{ae}_{\beta}$), and the Pitt-Peters model.

The first four represent on-axis responses of the vehicle, whereas the fifth is representative of the cross-coupling typical of helicopter dynamics (due to the lack of symmetry in the xz plane). In the range of frequency examined, the most relevant discrepancies among the predictions from the different wake inflow models, are in the region of the low-damped/unstable flight dynamics poles (*i.e.* 0.1 Hz). It is worth noting that, the presence of a stability augmentation system is expected to reduce the differences between the transfer function, due to the increase of mode

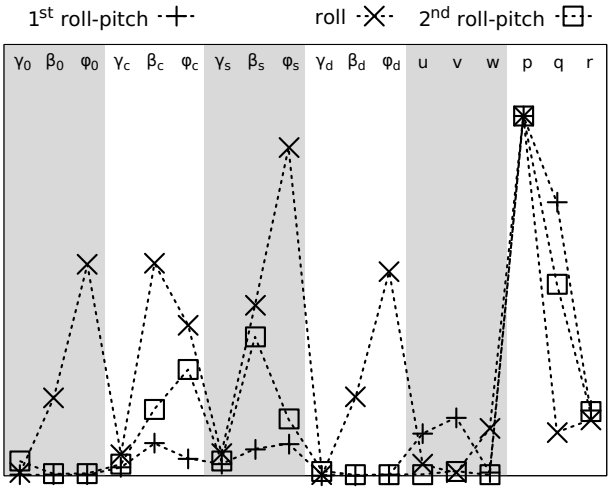

Figure 7: Eigenvectors associated to the poles in Fig. 5.

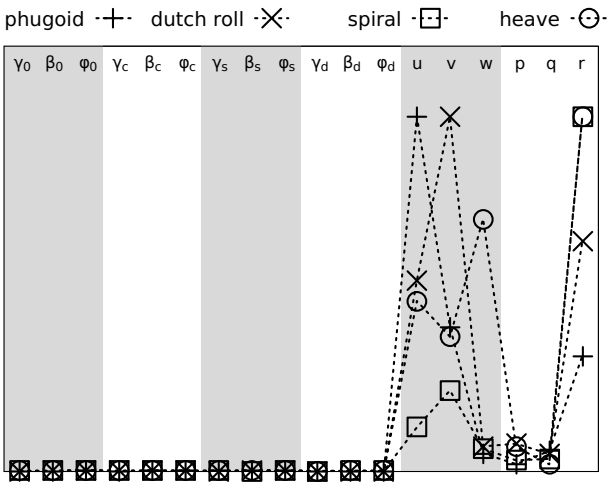

Figure 8: Eigenvectors associated to the poles in Fig. 6.

damping.

In some cases (w vs θ_0 and r vs θ_p), the kinematic-based inflow model produces different responses far from poles, as well. This is expected, since the kinematic model takes into account phenomena that are neglected by loads-based models like, for instance, the deformation of the rotor wake due to the motion of trailing edge [4].

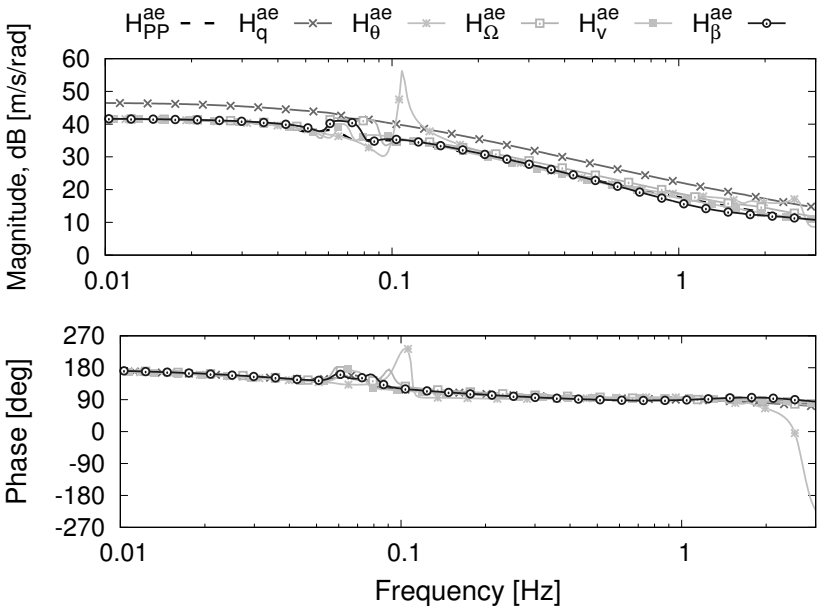

Figure 9: Transfer function w vs θ_0.

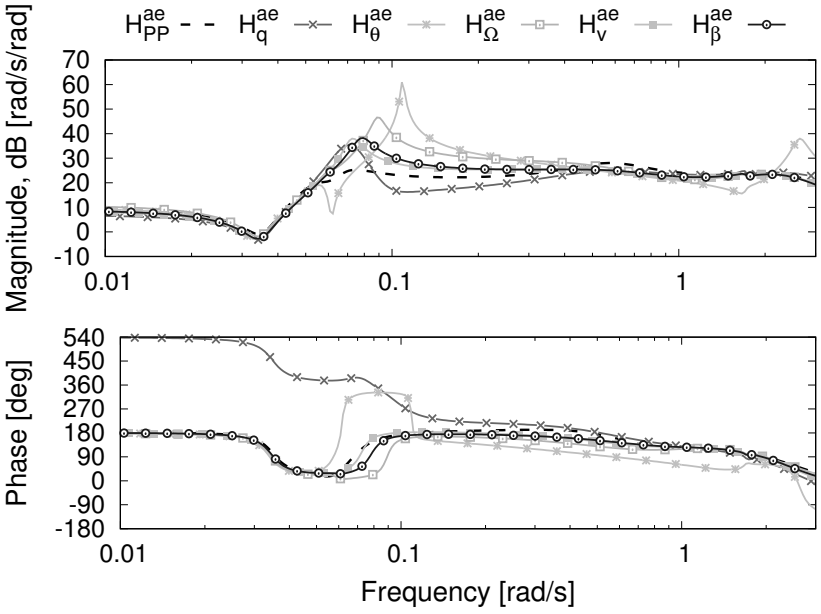

Figure 10: Transfer function p vs θ_c.

5 CONCLUSIONS AND FUTURE WORK

From the application to rotorcraft aeromechanics of the two introduced state-space wake inflow models extracted from a high-fidelity aerodynamic solver (relating inflow to kinematic variables and rotor loads, respectively), the following conclusions are drawn:

- For the linear inflow distribution considered (resembling that used in the Pitt-Peters model), the transfer functions are accurately approximated by introduction of few low-frequency poles.
- The loads-based model is not unique: indeed it is strongly dependent on the type of perturbation through which it is derived.
- The stability margin and the overall set of aeromechanics poles are significantly affected

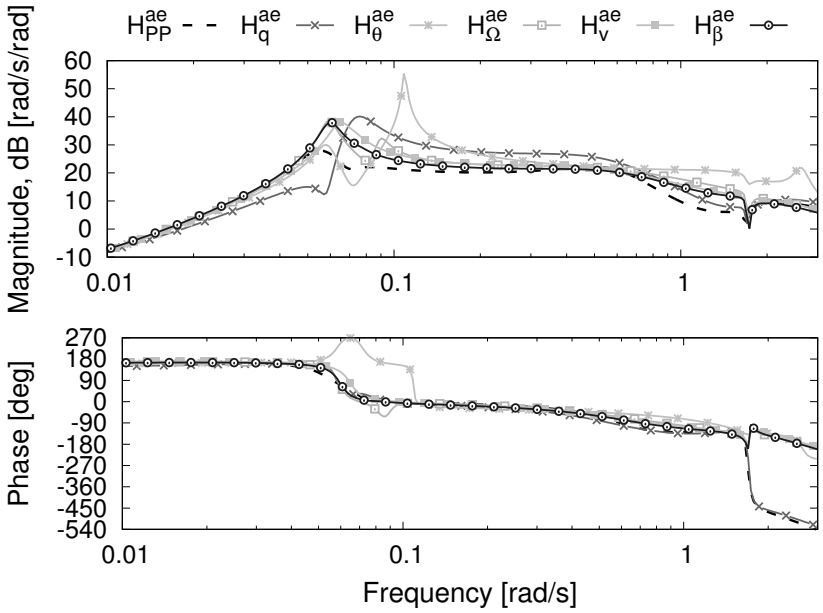

Figure 11: Transfer function q vs θ_s.

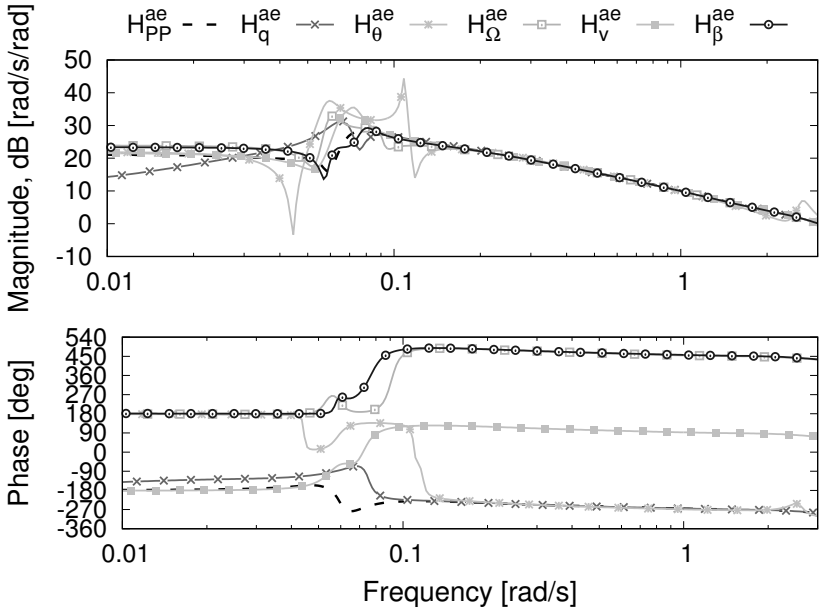

Figure 12: Transfer function r vs θ_p.

by dynamic inflow models applied.

- Helicopter responses to controls are strongly affected by inflow modeling, particularly close to the low-frequency, low-damped flight dynamic poles (namely phugoid and dutch-roll).

Additional investigations must be undertaken on the following topics:

- Improvement of inflow distribution approximation through increase of inflow coefficients (and consequently, load components for the loads-based model).
- Inclusion of purely kinematic effects in the loads-based model (like the motion of trailing edge), leading to the definition of a mixed kinematic-loads model.

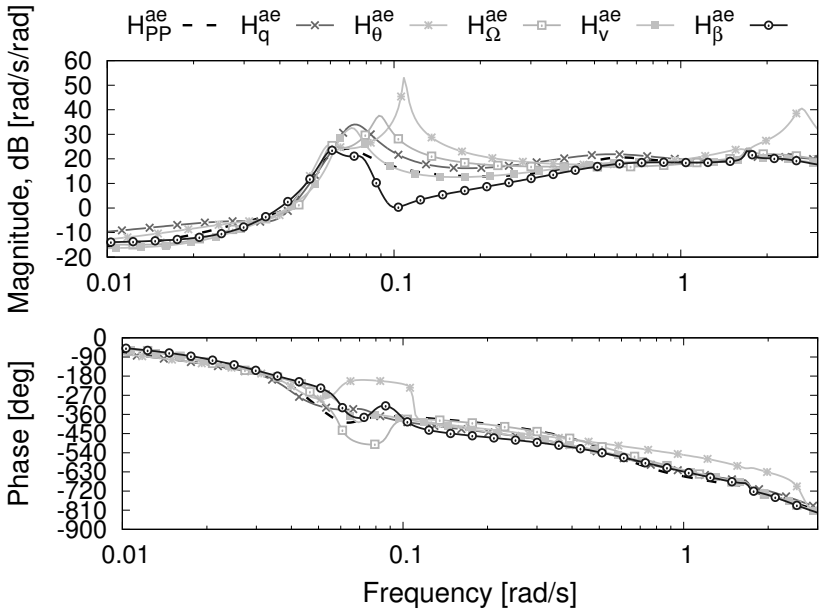

Figure 13: Transfer function p vs θ_s.

6 REFERENCES

[1] Peters, D. A., Barwey, D., and Su, A. (1994). An integrated airloads-inflow model for use in rotor aeroelasticity and control analysis. *Mathematical and computer modelling*, 19(3-4), 109–123.

[2] Pitt, D. M. and Peters, D. A. (1981). Theoretical Predictions of Dynamic Inflow Derivatives. *Vertica*, 5, 21–34.

[3] Pitt, D. M. and Peters, D. A. (1989). Comparison of measured induced velocities with results from a closed-form finite state wake model in forward flight. In *45th Annual Forum AHS, Boston, MA*. pp. 533–551.

[4] Arnold, U. T., Keller, J. D., Curtiss, H., et al. (1998). The effect of inflow models on the predicted response of helicopters. *Journal of the American Helicopter Society*, 43(1), 25–36.

[5] He, C., Lee, C., and Chen, W. (2000). Technical note: Finite state induced flow model in vortex ring state. *Journal of the American Helicopter Society*, 45(4), 318–320.

[6] Peters, D. A. and He, C. (2006). Technical note: Modification of mass-flow parameter to allow smooth transition between helicopter and windmill states. *Journal of the American Helicopter Society*, 51(3), 275–278.

[7] Murakami, Y. and Houston, S. (2008). Dynamic inflow modelling for autorotating rotors. *The Aeronautical Journal*, 112(1127), 47–53.

[8] Brown, R. E., Line, A. J., and Ahlin, G. A. (2004). Fuselage and tail-rotor interference effects on helicopter wake development in descending flight. In *60th Annual Forum of the American Helicopter Society, Baltimore, MD, USA*, vol. 710.

[9] Fanciullo, T., Zhao, J., Prasad, J., et al. (2000). Simulation of finite-state dynamic inflow models for in-ground effect & maneuvering flight conditions. In *AEROMECHANICS 2000- American Helicopter Society Aeromechanics Specialists' Meeting*.

[10] Rand, O., Khromov, V., Hersey, S., et al. (2015). Linear inflow model extraction from high-fidelity aerodynamic models for flight dynamics applications. In *71 ANNUAL FORUM PROCEEDINGS-AMERICAN HELICOPTER SOCIETY*. AMERICAN HELICOPTER SOCIETY, INC.

[11] Gennaretti, M., Gori, R., Serafini, J., et al. (Dallas, TX, June 2015). Rotor Dynamic Wake Inflow Finite-State Modelling. *33rd AIAA Applied Aerodynamics Conference*.

[12] Gennaretti, M., Gori, R., Serafini, J., et al. Identification of rotor wake inflow finite-state models for flight dynamics simulations. *CEAS Aeronautical Journal*, 8(1), 1–22.

[13] Cardito, F., Gori, R., Bernardini, G., et al. (2015). Finite-state dynamic wake inflow modelling for coaxial rotors. In 41^{st} *European Rotorcraft Forum*. Munich, D.

[14] Cardito, F., Gori, R., Bernardini, G., et al. (2016). Identification of coaxial-rotors dynamic wake inflow for flight dynamics and aeroelastic applications. In *42nd European Rotorcraft Forum*.

[15] Gennaretti, M., Pasquali, C., Cardito, F., et al. (2017). Dynamic wake inflow modeling in ground effect for flight dynamics applications. In *American Helicopter Society International 73rd Annual Forum*.

[16] Gennaretti, M., Gori, R., Cardito, F., et al. (2016). A space-time accurate finite-state inflow model for aeroelastic applications. In *American Helicopter Society International 72nd Annual Forum*.

[17] Pitt, D. M. and Peters, D. A. (1983). Rotor dynamic inflow derivatives and time constants from various inflow models. In *15th European Rotorcraft Forum: September 13-15, 1983, Stresa, Italy*.

[18] Gori, R., Serafini, J., Molica Colella, M., et al. (2016). Assessment of a state-space aeroelastic rotor model for rotorcraft flight dynamics. *CEAS Aeronautical Journal*, 7(3), 405–418. ISSN 1869-5590. doi:10.1007/s13272-016-0196-1.

[19] Pavel, M., Jump, M., and Dang-Vu, B. (2013). Adverse rotorcraft pilot couplingsâĂŤpast, present and future challenges. *Progress in Aerospace*, 62, 1–51. ISSN 03760421. doi: 10.1016/j.paerosci.2013.04.003.

[20] Pavel, M. D., Masarati, P., Gennaretti, M., et al. (2015). Practices to identify and preclude adverse Aircraft-and-Rotorcraft-Pilot Couplings–A design perspective. *Progress in Aerospace Sciences*, 76, 55–89.

[21] Gennaretti, M., Serafini, J., Masarati, P., et al. (2013). Effects of Biodynamic Feedthrough in Rotorcraft/Pilot Coupling: Collective Bounce Case. *Journal of Guidance, Control, and Dynamics*, 36(6), 1709–1721. ISSN 0731-5090. doi:10.2514/1.61355.

[22] Serafini, J., Colella, M. M., and Gennaretti, M. (2014). A finite-state aeroelastic model for rotorcraft–pilot coupling analysis. *CEAS Aeronautical Journal*, 5(1), 1–11.

[23] Gennaretti, M. and Bernardini, G. (2007). Novel boundary integral formulation for blade-vortex interaction aerodynamics of helicopter rotors. *AIAA Journal*, 45(6), 1169–1176.

[24] Bendat, J. S. and Piersol, A. G. (2011). *Random data: analysis and measurement procedures*, vol. 729. John Wiley & Sons.

COPYRIGHT STATEMENT